HEAT TRANSFER ENGINEERING
https://doi.org/10.1080/01457632.2023.2191440

Taylor & Francis
Taylor & Francis Group

Heat Transfer Characteristics of CO_2 in a Horizontal Tube under Subcritical and Supercritical Pressures

Chengrui Zhang[a], Bingtao Hao[a], Liangyuan Cheng[a], Jinliang Xu[a,b], and Qingyang Wang[a,b]

[a]Beijing Key Laboratory of Multiphase Flow and Heat Transfer for Low Grade Energy Utilization, North China Electric Power University, Beijing, China; [b]Key Laboratory of Power Station Energy Transfer Conversion and System of the Ministry of Education, North China Electric Power University, Beijing, China

ABSTRACT

Supercritical CO_2 heat transfer in vertical tubes has been widely studied, but limited work exists for that in horizontal tubes. In this work, experiments were conducted for CO_2 in a horizontal tube with inner diameter of 8 mm under wide range of pressures (5.51–20.41 MPa), covering both subcritical and supercritical conditions. The ranges of heat flux and mass flux were 97.5–404.0 kW/m^2 and 510.2–1314.2 kg/m^{2}s, respectively. The heat transfer for subcritical pressure far below critical pressure showed typical flow boiling characteristics, with a wall temperature peak along the tube corresponding to departure from nucleate boiling. For near-critical pressure, it showed characteristics similar to supercritical heat transfer, with continuous increase of wall temperature along the tube. The effects of different parameters including pressure, mass flux, and heat flux on the heat transfer behavior were analyzed and discussed. Moreover, using the pseudo-vapor quality concept of the supercritical three-regime-model introduced in a previous work, the heat transfer coefficient was found to behave very similarly between subcritical and supercritical conditions. The experimental results showed significant deviation from single-phase convection within the two-phase/two-phase-like region compared with the single-phase regions, and which validates the similarity between subcritical boiling and supercritical pseudo-boiling.

Introduction

Supercritical fluids have been widely used in a variety of applications including food processing, separation and purification, and materials synthesis [1, 2]. Supercritical CO_2 (sCO_2) is attracting significant interests. Due to the high global warming potential of the traditional refrigerants such as R22, R32 and R134a, CO_2 as a natural refrigerant is considered an alternative, and trans-critical CO_2 cycles have been applied in vehicle and residential air conditioning and industrial refrigeration [3, 4]. For power generation, supercritical CO_2 Brayton cycles have higher efficiency, more compactness, and better flexibility than traditional water steam cycles, and is thus widely studied for solar thermal, fossil fuel, and nuclear power plants [5]. Investigation of the heat transfer characteristics of sCO_2 in tubes can provide guidance for the design and operation of these cycles and is thus important for refrigeration and power generation applications.

Experimental investigations of sCO_2 heat transfer in tubes have been carried out quite extensively [6]. However, most of the work focused on heat transfer of sCO_2 flowing in vertical tubes, either upward or downward. For sCO_2 heat transfer in horizontal tubes, there are only limited amounts of available literature. Adebiyi and Hall [7] studied heat transfer of sCO_2 at 7.6 MPa in a horizontal tube with inner diameter of 22.14 mm under different mass flux, heat flux and inlet temperature conditions. They found that the bottom generatrix has better heat transfer than the top generatrix due to the buoyancy effect. Tanimizu and Sadr [8] studied the effect of buoyant force on convective heat transfer of sCO_2 in a horizontal tube with tube inner diameter of 8.7 mm, pressure of 7.5–9 MPa, mass flow rate of 0.011–0.017 kg/s, heat flux of 16–64 kW/m^2, and fluid inlet temperature of 24–28 °C. The results show that three buoyancy parameters proposed in previous literature are not applicable to their experimental results. Wang et al. [9] studied the pressure drop characteristics of sCO_2 in microtubes with

CONTACT Associate Professor Qingyang Wang wangqy@ncepu.edu.cn Beijing Key Laboratory of Multiphase Flow and Heat Transfer for Low Grade Energy Utilization, North China Electric Power University, Beijing 102206, China.

Nomenclature

Bo	boiling number
c_p	specific heat capacity, J/(kg·K)
d	tube diameter, m
DB	Dittus-Boelter correlation
e_A	mean relative error
e_R	mean absolute relative error
e_S	root-mean-square relative error
g	gravitational acceleration, m/s^2
G	mass flux, kg/m^{2}s
h	heat transfer coefficient, W/m^2·K
i	enthalpy, kJ/kg
I	heating current, A
k	turbulent kinetic energy, m^2/s^2
K	supercritical *K* number
L	length, m
$\dot{m}$	mass flow rate, kg/s
Nu	Nusselt number
P	pressure, Pa
Pr	Prandtl number
Q	heat transfer rate, W
q	wall heat flux, W/m^2
Re	Reynolds number
SBO	supercritical boiling number
SST	shear stress transport
Se	secondary flow number
T	temperature, K or °C
U	heating voltage, V
x	thermodynamic equilibrium vapor quality or pseudo-vapor quality
z	axial location, m

Greek symbols

ΔP	pressure drop, Pa
λ	thermal conductivity, W/mK
μ	dynamic viscosity, Pa·s
ω	vorticity, 1/s
ρ	density, kg/m^3

Subscripts

ave	average
b	bulk fluid
bottom	bottom generatrix
c	critical point
exp	experiment
i	inner wall
in	inlet
L	saturated liquid
LL	liquid-like
o	outer wall
out	outlet
pc	pseudo-critical point
side	side generatrix
top	top generatrix
V	saturated vapor
VL	vapor-like
w	inner wall condition

diameters of 0.5, 0.75 and 1 mm under experimental pressures of 7.6, 8.0 and 8.5 MPa and mass flux of 58.1 and 78.2 kg/m^2 s, and found that the pressure drop increases with the increase of mass flow rate and inlet temperature, and decreases with the increase of pressure and diameter. The acceleration pressure drop becomes very important with the increase of tube diameter, and the frictional pressure drop plays a dominant role for small tube diameter. The existing empirical correlations for friction factor can predict the frictional pressure drop with a relative error of about 30%. Kim et al. [10] studied the effect of buoyancy for sCO_2 flow in a horizontal tube with experimental conditions covering pressure of 7.587–7.735 MPa, mass flux of 64.1–250.5 kg/m^2 s, heat flux of 3.1–25.9 kW/m^2, and inlet temperature of 30 °C. Buoyancy parameters were introduced, and it is found that the heat transfer characteristics along the flow direction are greatly affected by the acceleration effect and have little to do with buoyancy force.

There are also several numerical studies reported in the literature for sCO_2 heat transfer in horizontal tubes [6]. Wang et al. [11] carried out numerical simulation on the convective heat transfer of sCO_2 in a large diameter tube corresponding to the experimental conditions of Adebiyi and Hall [7]. They found that the secondary flow caused by the buoyancy effect changes the sCO_2 flow field, and thus the turbulent distribution is also changed, resulting in different heat transfer coefficient of sCO_2 along the circumferential direction and consequently a large temperature difference between the top and bottom walls. Chu and Laurien [12] studied the heat transfer characteristics of sCO_2 in a small diameter tube through direct numerical simulation, and found that flow stratification occurs in the tube flow, which is attributed to buoyancy effect. Due to the secondary flow generated by density difference, the fluid with lower density and higher temperature gathers at the top of the tube, so that the wall temperature at the top generatrix is much higher than at the bottom generatrix. Zhang et al. [13] used shear stress transport (SST) k-ω turbulence model to study the convective heat transfer characteristics of sCO_2 in a horizontal tube under circumferential non-uniform heat flux. The results show that in most cases, the circumferential non-uniform heat flux negatively affects the heat transfer of sCO_2, and the overall heat transfer performance depends on

the heat transfer at the top of the tube. It is also shown that the ratio of the secondary flow number to the Reynolds number *Se/Re* can accurately predict the influence of buoyancy effect on the local heat transfer performance of sCO_2 in non-uniformly heated horizontal tubes. Yan and Xu [14] also used SST k-ω turbulence model to study the heat transfer of sCO_2 in a horizontal tube. They found that the flow and heat transfer characteristics are similar to subcritical gas-liquid two-phase flow and attributed the difference in circumferential distribution of wall temperature to the gas-like film thickness, gas-like film properties and turbulent kinetic energy.

In most of the existing studies, supercritical fluid is basically treated as single-phase fluid. However, the heterogeneous feature of supercritical fluid has been acknowledged in the recent decades. Gallo et al. [15] studied supercritical water using molecular dynamics simulation and found that the dynamic and thermodynamic properties show a crossover from liquid-like to gas-like behaviors when crossing the Widom line. Through X-ray scattering and molecular dynamics simulation, Simeoni et al. [16] observed sharp transition from liquid-like to gas-like fluid when crossing the Widom line. Maxim et al. [17, 18] observed sharp density variation from liquid-like to gas-like supercritical water using neutron imaging. Using thermodynamic analysis, Banuti [19] proposed the calculation method for the transition temperatures when crossing the Widom line from liquid-like to gas-like regions. Ha et al. [20] found the existence of a Widom delta through machine learning method where gas-like and liquid-like molecules coexist. Because of the supercritical two-phase feature, the pseudo-boiling concept is being considered to understand supercritical heat transfer. Zhu et al. [21] first connected pseudo-boiling with the abnormal phenomena of heat transfer deterioration of sCO_2 in tubes, and proposed a supercritical boiling number *SBO* in analogous to subcritical boiling number. They found that the *SBO* number can be used as the transition criterion to distinguish heat transfer deterioration and normal heat transfer. Zhu et al. [22] subsequently proposed a supercritical K number, and developed a heat transfer correlation using this K number, which can be used to accurately predict the heat transfer of various supercritical fluids under wide range of working conditions. Wang et al. [23] systematically compared supercritical pseudo-boiling and subcritical boiling, and proposed a three-regime-model for supercritical pseudo-boiling, establishing the first theoretical framework for pseudo-boiling.

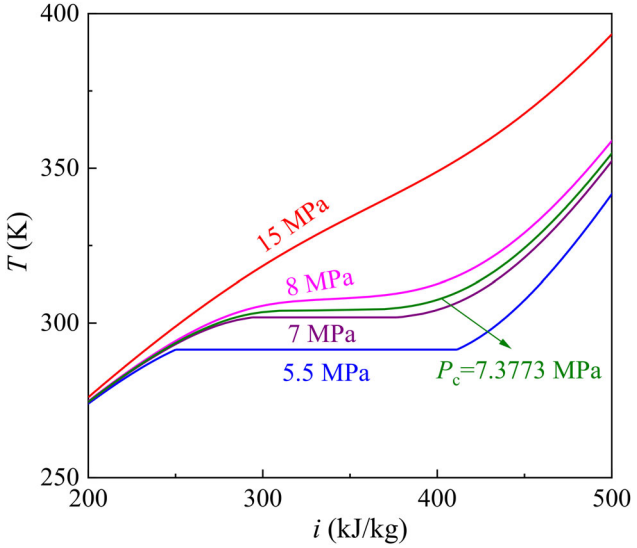

Figure 1. The temperature-enthalpy (T-i) curves for CO_2 at different pressures.

There are significantly different characteristics between subcritical boiling and supercritical pseudo-boiling. The most notable difference is that there is gas-liquid interface in subcritical boiling heat transfer, while this interface disappears for supercritical pseudo-boiling. Figure 1 shows the temperature-enthalpy (T-i) curves for CO_2 under both sub- and supercritical pressures, where the subcritical curves have a horizontal flat segment corresponding to liquid-vapor coexistence line, and the supercritical curves varies continuously with temperature. Nevertheless, under supercritical pressures, drastic variations of fluid properties including density ρ, specific heat capacity c_p, thermal conductivity λ and viscosity μ enable the division of supercritical fluid domain into gas-like and liquid-like regions. Therefore, some aspects of supercritical pseudo-boiling are very similar to subcritical boiling. Comparing supercritical heat transfer with subcritical heat transfer could provide insights into the underlying mechanisms of supercritical heat transfer.

For subcritical flow boiling, Yun et al. [24] found the heat transfer coefficient increased significantly with increasing heat flux when the vapor mass quality is small, but after the dry-out point, the influence of heat flux on the heat transfer coefficient is greatly reduced, and the influence of mass flux on the heat transfer coefficient is opposite to that of heat flux. Ducoulombier et al. [25] found three different heat transfer behaviors of CO_2 flow boiling: when $x < 0.1$, the heat transfer coefficient was mainly affected by heat flux; with large vapor mass quality, it is found that when the boiling number $Bo > 1.1 \times 10^{-4}$, the heat transfer coefficient is not only strongly affected

by heat flux and moderately affected by mass flux. While when $Bo < 1.1 \times 10^{-4}$, the effect of heat flux on heat transfer coefficient is negligible while the effect of mass flux is significant. Cheng et al. [26–28] modified the Cheng-Ribatski-Wojtan-Thome heat transfer model and proposed a new CO_2 flow pattern map. In addition, they also updated the flow boiling heat transfer correlation in dry-out region based on CO_2 data and developed a general flow boiling heat transfer model suitable for CO_2 horizontal pipe, with applicable experimental conditions covering tube diameter of 0.6–10 mm, mass flux of 50–1500 kg/m^{2}s, heat flux of 1.8–46 kW/m^2, and reduced pressures of 0.21–0.87. Jiang et al. [29] studied the characteristics of dry-out in the flow boiling of CO_2 in horizontal mini-channels and found that with increasing heat flux, nucleate boiling is enhanced but dry-out occurs earlier.; With increasing mass flux, the vapor mass quality at initial dry-out is reduced, and the heat transfer coefficient in the later stage of dry-out is increased. In addition, with higher the saturation temperature, the dry-out phenomenon is more likely to occur.

There have been several works reporting the comparison between supercritical and subcritical heat transfer. Gang et al. [30] experimentally studied the heat transfer characteristics of subcritical and supercritical water in an upward inclined circular tube under heating conditions. The effects of pressure and heat flux were discussed for subcritical, near critical, and supercritical conditions. Wang et al. [31] studied the characteristics of water heated in a downward inclined tube, and observed deteriorated heat transfer near the top of the tube, due to dry-out and departure from nucleate boiling for subcritical pressures and due to buoyancy effect for supercritical pressures. Zhu et al. [32] experimentally studied the heat transfer characteristics of water in a vertical upward tube. They found that heat transfer deterioration is caused by dry-out for subcritical pressures and by departure from nucleate boiling for near-critical pressures, and that both enhanced and deteriorated heat transfer occur for supercritical pressures. Wang et al. [33] studied the heat transfer characteristics of subcritical and supercritical water in vertical upward tubes, and found that the mechanism for heat transfer deterioration under supercritical pressures is similar to the departure from nucleate boiling under subcritical pressures. For CO_2, Lei et al. [34] conducted experimental comparison of heat transfer under subcritical and supercritical conditions, and discussed the effects of different parameters.

From the discussions above, it can be concluded that despite extensive efforts to study heat transfer characteristics of sCO_2 in vertical tubes, limited experimental studies exist for sCO_2 heat transfer in horizontal tubes. Moreover, at present, subcritical heat transfer and supercritical heat transfer are mostly discussed separately, and a systematic comparison between their heat transfer characteristics is needed, especially for CO_2. In this article, we conduct experiments for sCO_2 heated in a horizontal tube with inner diameter of 8 mm, covering wide ranges of parameters including pressure (5.51–20.41 MPa), mass flux (510.2–1314.2 kg/m^{2}s), and heat flux (97.5–404.0 kW/m^2). Notably, the pressure range covers both subcritical and supercritical pressures. The effects of pressure, heat flux and mass flux on the heat transfer characteristics of CO_2 at subcritical and supercritical pressures are studied. The subcritical and supercritical heat transfer characteristics are also compared and discussed. Moreover, based on the subcritical vapor quality and the supercritical pseudo-vapor quality (defined in Ref. [23]), it is shown that under subcritical and supercritical conditions, sCO_2 heat transfer in a horizontal tube behaves similarly, confirming the validity of the supercritical three-regime-model.

Experimental

Experimental system

Figure 2 shows the schematic of the experimental system, which is adapted from the one used in Ref. [35] by varying the orientation of the test section. The system consists of the CO_2 circulation system, the coolant circulation system, the heating system, and the data acquisition system. The CO_2 fluid is initially stored in the storage tank. During experiments, it is pressurized by the high-pressure pump and charged into the circulation loop, then flows through the mass flow meter for mass flow rate measurement, passes the preheater to be heated to designed inlet temperature condition, enters the test section for experiments, flows through the cooler to return to liquid state, and finally returns to the pump. Details about the experimental system can be found in Ref. [35].

Test section

Figure 3 shows the schematic of the test tube. The center part of the test tube is heated using direct current heating. Copper electrodes are directly welded on the stainless-steel test tube at both ends of the tube,

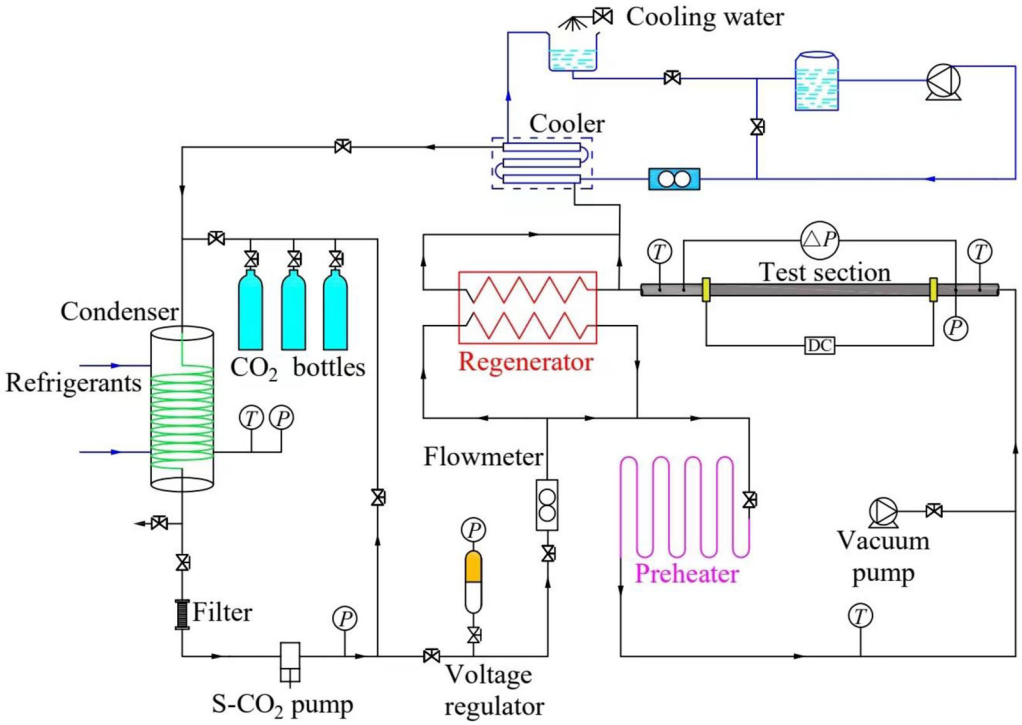

Figure 2. Schematic of the experimental system.

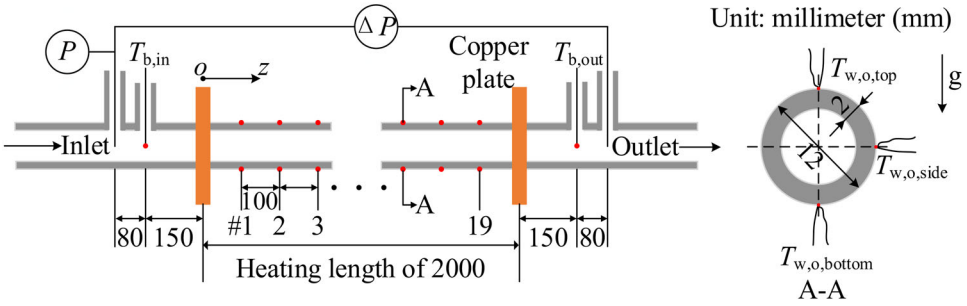

Figure 3. Schematic of the test tube and the temperature measurement positions.

and a low-voltage, large-current direct current is applied to generate joule heating in the tube wall and provide a uniform heat flux. The experimental test tube is made of 1Cr18Ni9Ti stainless-steel with an inner diameter of 8 mm and a wall thickness of 2 mm as shown in Figure 3. The total length of the test tube is 3600 mm, of which the total length of the heating section is 2000 mm, and there are 800 mm flow stabilization sections before and after the heating section. Two sheathed thermocouples are inserted into the center of the tube before and after the heating section to measure the inlet and outlet temperatures. A pressure gauge and a differential pressure transducer are arranged to measure the inlet pressure and the pressure drop across the heating section, as shown in Figure 3. K-type thermocouples are welded on the tube outer surface of the heating section for wall temperature measurement. A total of 19 temperature measurement positions along the tube are arranged 100 mm apart, and three thermocouples are welded at the top, side, and bottom generatrixes for each measurement positions, as shown in Figure 3. Thermal insulation material of 50 mm thick is wrapped outside of the test section to prevent heat loss to the ambient.

Data reduction

In this work, we employ a data reduction method similar to the one reported in Ref. [35]. From the measured quantities including the mass flow rate $\dot{m}$, the inner tube diameter d_i, the inlet and outlet temperatures $T_{b,in}$ and $T_{b,out}$, tube heating length L, and the outer tube wall temperatures T_w, the other quantities are calculated as follows.

The mass flux is calculated as

$$G = \frac{\dot{m}}{\frac{1}{4}\pi d_i^2} \tag{1}$$

The total heating power is calculated by

$$Q = \dot{m}(i_{b,out} - i_{b,in}) \tag{2}$$

where the inlet and outlet fluid enthalpy $i_{b,in}$ and $i_{b,out}$ are obtained based on the inlet and outlet bulk fluid temperatures $T_{b,in}$ and $T_{b,out}$, respectively.

The inner wall heat flux is calculated as

$$q = \frac{Q}{\pi d_i L} \tag{3}$$

The bulk fluid enthalpy at axial position z is calculated as

$$i_b(z) = i_{b,in} + \frac{\pi q d_i z}{\dot{m}} \tag{4}$$

The corresponding bulk temperature is then obtained from the working pressure and the bulk fluid enthalpy using the NIST software [36].

Assuming uniform heating, the inner wall temperatures on the top, side, and bottom can be obtained according to the solution for one-dimensional heat conduction in the radial direction with internal heat source, expressed as

$$T_{w,i} = T_{w,o} - \left[\frac{q d_i}{4\lambda}\frac{\left(\frac{d_i}{d_o}\right)^2 - 2\ln\left(\frac{d_i}{d_o}\right) - 1}{1 - \left(\frac{d_i}{d_o}\right)^2}\right] \tag{5}$$

The temperature-dependent thermal conductivity of stainless-steel can be represented by

$$\lambda = \lambda_0 + \alpha \times T_w \tag{6}$$

where $\lambda_0 = 14.3$ W/mK is the room temperature thermal conductivity and $\alpha = 0.01475$ W/mK^2 is the temperature coefficient, and the wall temperature T_w has a unit of °C. The T_w in Eq. (6) should be evaluated as the average temperature between $T_{w,i}$ and $T_{w,o}$. However, for the current experimental conditions, evaluating T_w as $T_{w,o}$ instead of the average temperature makes negligible difference in the calculated $T_{w,i}$. Therefore, to simplify calculation, $T_{w,o}$ is directly used in Eq. (6).

In Figure 3, due to the symmetry against the vertical centerline, it is assumed that the wall temperature on the left side is equal to that on the right side. Therefore, the average inner wall temperature for each axial position is calculated as

$$T_{w,i,ave} = \frac{T_{w,i,top} + T_{w,i,bottom} + T_{w,i,side}}{3} \tag{7}$$

where the subscripts top, bottom, and side represent different generatrix locations (see Figure 3).

Finally, the local heat transfer coefficient and the circumferential average heat transfer coefficient are both calculated as

$$h = \frac{q}{T_{w,i} - T_b} \tag{8}$$

For local heat transfer coefficient, the local inner wall temperature is used; while for average heat transfer coefficient, the average inner wall temperature is used.

The uncertainties of both directly measured and derived parameters are listed in Table 1. Detailed uncertainty analysis can be found in our previous publication [35].

Table 1. Main parameters and uncertainties.

Parameter	Range	Uncertainty
Pressure P (MPa)	5.51–20.41	1.30%
Mass flux G (kg/m^{2}s)	510.2–1314.2	2.05%
Heating voltage U (V)	10.6–23.4	0.75%
Heating current I (A)	444–883	1.35%
Heating power Q (kW)	4.90–20.33	1.54%
Heat flux q (kW/m^2)	97.5–404.0	4.61%
Inlet temperature $T_{b,in}$ (°C)	8.28–26.64	0.5 °C
Outlet temperature $T_{b,out}$ (°C)	20.77–245.47	0.5 °C
Wall temperature T_w (°C)	21.10–462.35	0.5 °C
Heat transfer coefficient h (kW/m^{2}K)	0.48–39.90	6.80%
Vapor quality x	−2.54–4.60	3.63%

Repeatability validation

To verify the reliability of the experimental system, we performed a set of repeating experiments, as shown in Figure 4. For experiments carried out on different days with the same working conditions, the wall

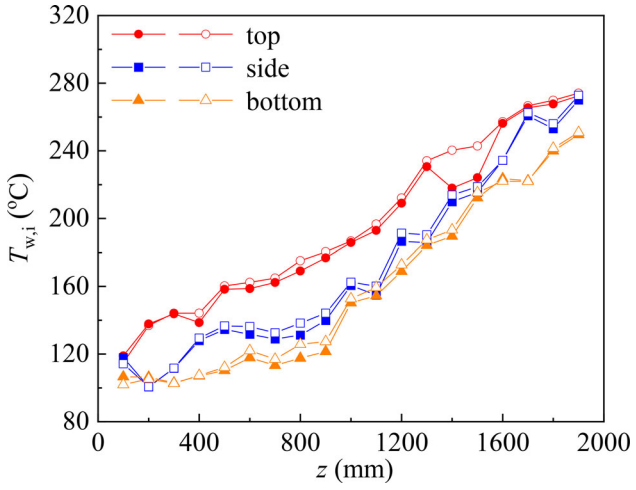

Figure 4. Wall temperature curves for the repeating experiments. Hollow symbols represent the first experiment with $P = 10.08$ MPa, $G = 750.9$ kg/m^{2}s, $q = 203.0$ kW/m^2. Solid symbols represent the second experiment with $P = 10.04$ MPa, $G = 753.5$ kg/m^{2}s, $q = 199.6$ kW/m^2.

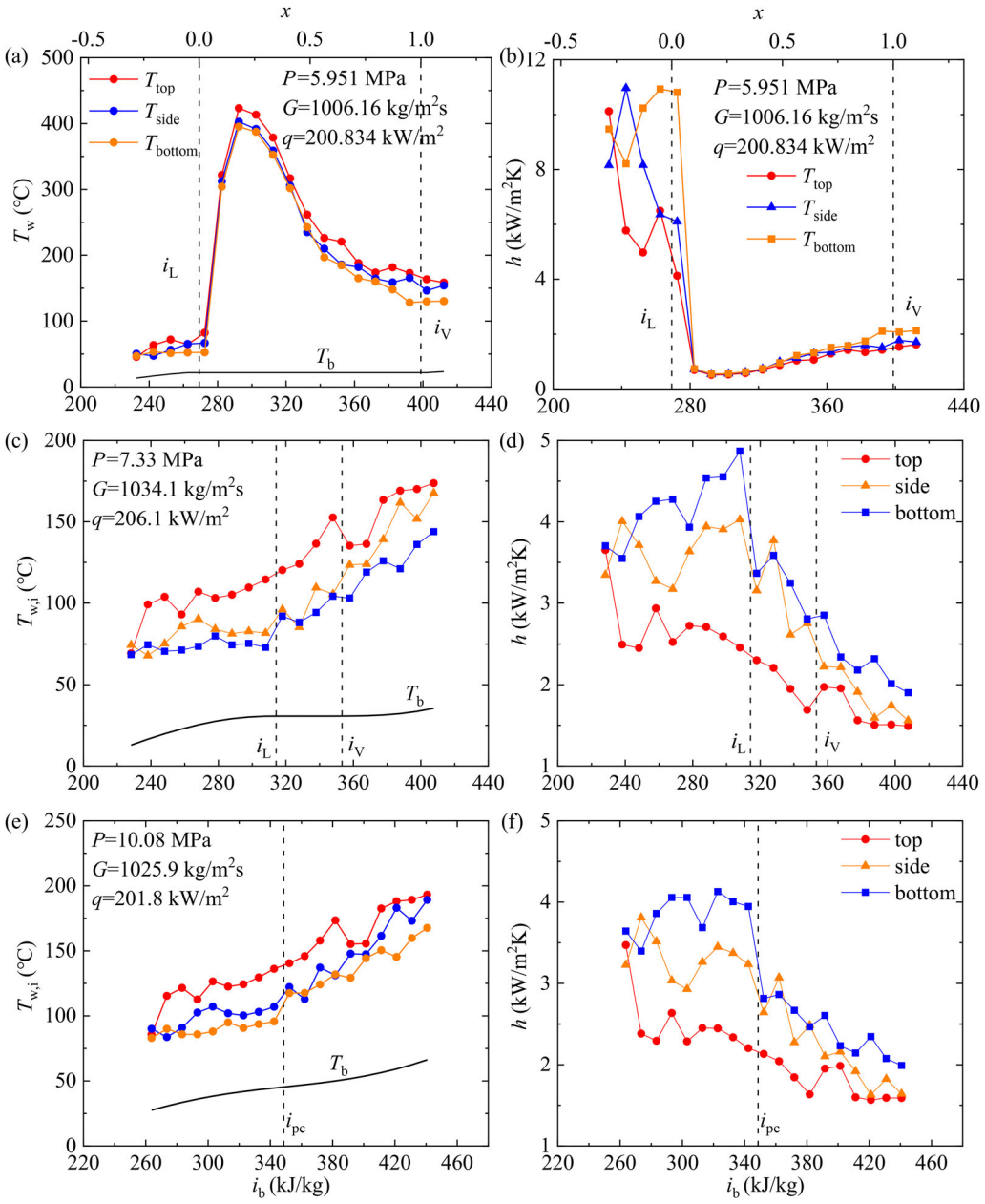

Figure 5. Heat transfer characteristics for three typical pressures: (a) and (b) subcritical, (c) and (d) near-critical, and (e) and (f) supercritical.

temperature curves for top, side and bottom of the horizontal tube are almost the same (except two thermocouples No. 14 and 15 at the top generatrix, due to possible welding problem), indicating that the experimental system is reliable, and the experimental results are repeatable.

Result and discussion

In this work, the working conditions cover a pressure range of 5.51–20.41 MPa, a mass flux range of 510.2–1314.2 kg/m^{2}s, and a heat flux range of 97.5–404.0 kW/m^2. The inlet temperature is set as 10 °C for subcritical pressures and 25 °C for supercritical pressures. It is worth noting that in Figures 5–8, for a particular experimental condition, the subfigures for wall temperature and for heat transfer coefficient may seem to have inconsistent trends. The reason is that the scale of the vertical axis is different, which causes some features of the trend to be not very obvious.

Heat transfer characteristics

Figure 5a–f show the typical wall temperature curves and the corresponding heat transfer coefficient curves obtained in our experiments, with the abscissa being

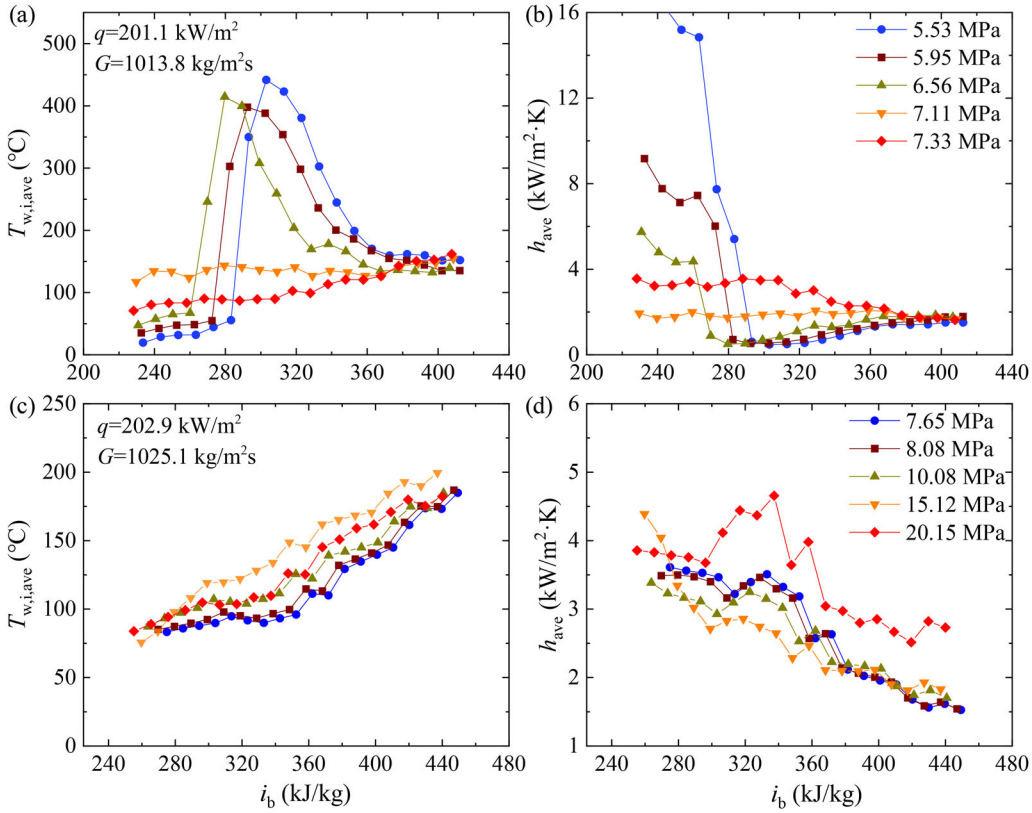

Figure 6. Variation of heat transfer characteristics with pressure for the same heat flux and mass flux.

the bulk fluid enthalpy i_b and the ordinate being the temperature or heat transfer coefficient at the corresponding position.

Figure 5a and b show the experimental results for pressure of 5.95 MPa, representing a typical subcritical case. The horizontal axis represents both the bulk fluid enthalpy (bottom) and the vapor quality (top). Generally, for a given axial position, the wall temperature increases from the bottom to the top in the circumferential direction, corresponding to the highest heat transfer coefficient at the bottom generatrix and the lowest heat transfer coefficient at the top generatrix. This can be attributed to the accumulation of vapor phase near the top of the tube due to the difference in densities of vapor and liquid phases, and the lower vapor thermal conductivity results in smaller heat transfer coefficient. Figure 5a and b also show the enthalpy corresponding to the saturated liquid and vapor phases by black dashed lines, corresponding to a vapor quality of 0 and 1, respectively. Near the inlet of the tube, the wall temperature slightly increases along the tube with small temperature difference between tube wall and bulk fluid, corresponding to large heat transfer coefficient over 5 kW/m^2K, which is within the same order of magnitude with the value reported in Ref. [24, 37, 38]. This segment of the curves represents subcooled boiling regime. As the fluid reaches saturation temperature, the curves enter saturated boiling regime. At a vapor quality of about 0.1, the wall temperature sharply increases to achieve a peak value of over 400 °C, after which the wall temperature decreases gradually, which corresponds to departure from nucleate boiling. When the bulk fluid enthalpy exceeds the saturated vapor enthalpy and the vapor quality exceeds 1, the heat transfer mode becomes superheated vapor convective flow. It can be seen that the sharp rise of wall temperature occurs when the fluid enters the two-phase region between the two black dashed lines. Correspondingly, the heat transfer coefficient drops sharply and then recovers gradually. The reason for the wall temperature peak is that as the fluid is heated along the tube, the vapor quality gradually accumulates, and to a certain location, departure from nucleate boiling occurs such that vapor films form near the tube wall to cause significantly deteriorated heat transfer. Before reaching the wall temperature peak, the main heat transfer mode is nucleate boiling (including subcooled boiling) with efficient heat transfer and high heat transfer coefficient. After the wall temperature peak, the heat transfer is dominated by vapor phase conduction, and the wall temperature decreases due to the increasing fluid thermal conductivity with increasing fluid temperature along the tube.

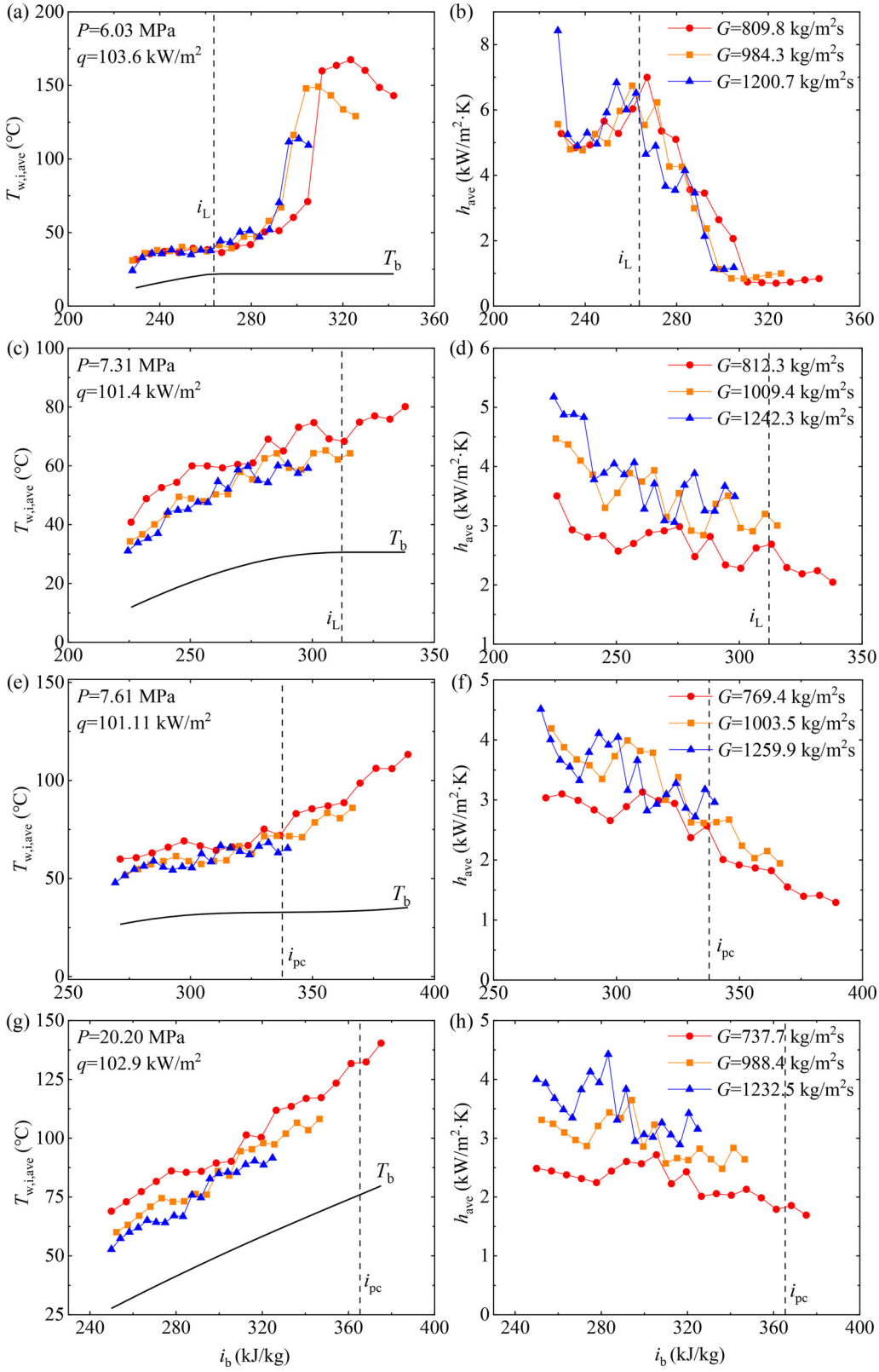

Figure 7. Variation of heat transfer characteristics with mass flux for the same heat flux and pressure.

Figure 5c and d show the experimental results for pressure of 7.33 MPa, representing a typical near-critical case, and Figure 5e and f show the experimental results for pressure of 10.08 MPa, representing a typical supercritical case. These two cases show very similar trend in their wall temperature and heat transfer coefficient. The wall temperature shows increasing circumferential trend from the bottom to the top,

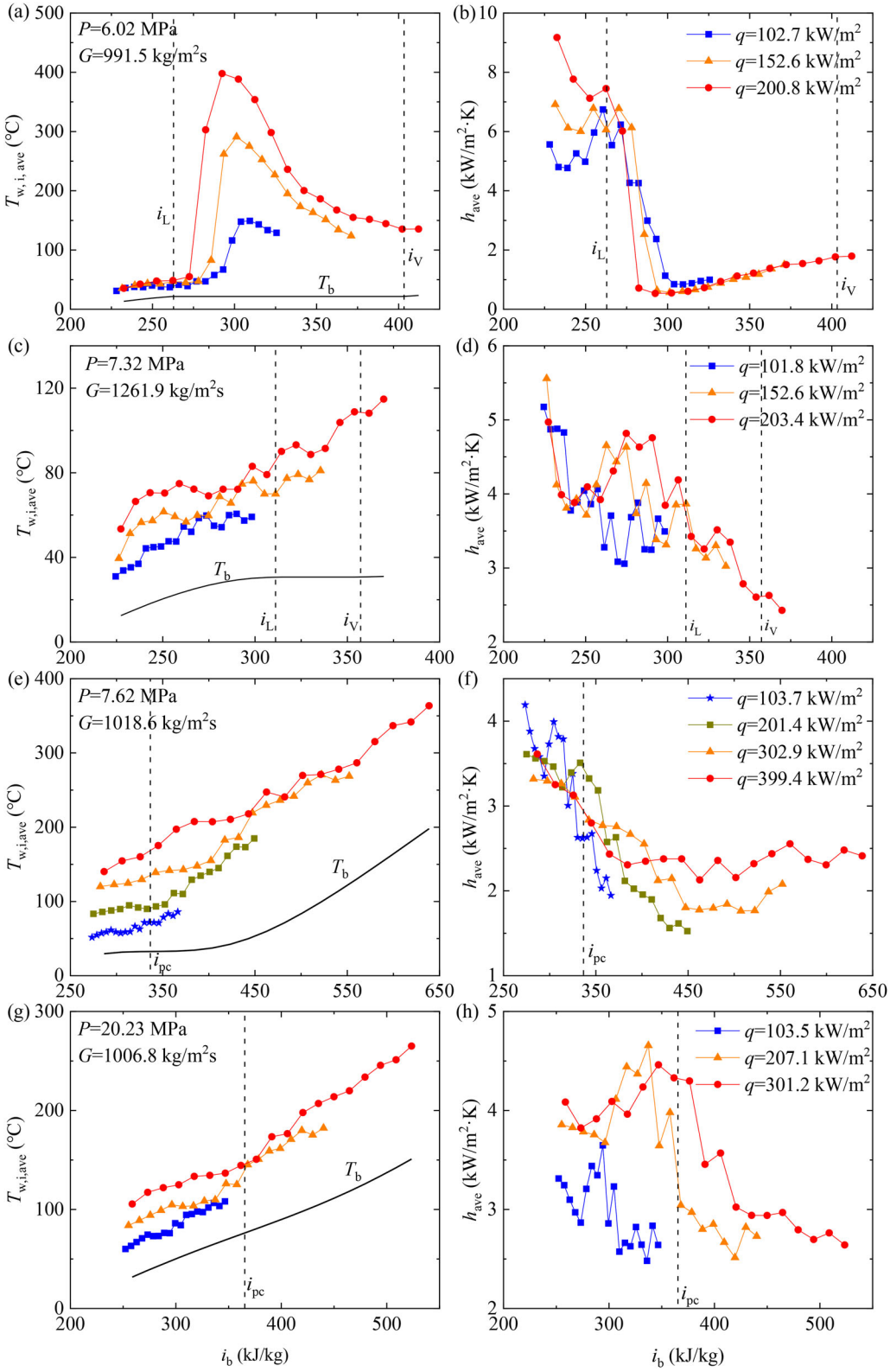

Figure 8. Variation of heat transfer characteristics with heat flux for the same mass flux and pressure.

with the top wall temperature being the highest at a given axial location, resulting in a decreasing heat transfer coefficient from the bottom generatrix to the top generatrix, similar to the subcritical case. The reason is also similar: fluid with lower density and lower thermal conductivity accumulates near the top part of the tube cross-section, while fluid with higher density and higher thermal conductivity accumulates

near the bottom, therefore results in higher wall temperature and lower heat transfer coefficient at the top than at the bottom. For near-critical case, the low-density and high-density fluids correspond to the vapor and liquid phases, respectively; while for supercritical case, they correspond to the gas-like and liquid-like fluids as mentioned before. The wall temperature generally increases along the tube, without the appearance of a notable temperature peak. For supercritical case, except near the inlet due to the entrance effect, the heat transfer coefficient increases slightly before reaching the pseudocritical point. This is due to the significantly large heat capacity of the fluid near the pseudocritical point enabling enhanced heat absorbing ability of the fluid. After the pseudocritical point, the heat transfer coefficient decreases gradually, due to the small variation of thermophysical properties. For near-critical case, the latent heat and the surface tension become very small, being 38.66 kJ/kg and 0.012 mN/m at 7.33 MPa, while the values are much higher at 5.95 MPa, attaining 142.67 kJ/kg and 1.00 mN/m, respectively [36]. Therefore, small bubbles are easily generated and coalesced into vapor films [39], and the significant heat transfer enhancement due to boiling is no longer dominant. The difference between liquid and vapor phases becomes small, and the heat transfer is very similar to the supercritical case.

Effects of pressure

Figure 6 shows the circumferential average wall temperature and heat transfer coefficient curves at different pressures, with Figure 6a and b showing subcritical conditions and Figure 6c and d showing supercritical conditions. The mass flux and heat flux are 1000 kg/m^{2}s and 200 kW/m^2, respectively.

For subcritical pressures shown in Figure 6a and b, the variation of wall temperature and heat transfer coefficient with pressures far from the critical pressure (5.51–6.56 MPa) is significantly different from that with near-critical pressures (7.04–7.33 MPa). Their typical characteristics and differences have been discussed before. For subcritical pressures far from the critical pressure, before the wall temperature peak corresponding to departure from nucleate boiling, the wall temperature increases, and the heat transfer coefficient decreases with increasing pressure. The position of the wall temperature peak also shifts toward left (smaller enthalpy) with increasing pressure, similar to the trend observed in Ref. [32] for water. These are because the latent heat and surface tension of the fluid decreases with increasing pressure toward critical pressure, so that in the regime where nucleate boiling dominates heat transfer, it is more difficult to retain the liquid film so that departure from nucleate boiling occurs more easily with increasing pressure [40]. For near-critical pressures, the wall temperature varies smoothly, and the heat transfer coefficient increases with increasing pressure, which is due to the increased heat capacity as the fluid approaches the critical pressure. In the large enthalpy region near the outlet of the tube, the heat transfer coefficient curves converge and do not vary too much with pressure, which is because the fluid state becomes vapor phase, and the physical properties are similar under different subcritical pressures.

For supercritical pressures shown in Figure 6c and d, the variation trends of wall temperature and heat transfer coefficient are similar among different pressures. Generally, the wall temperature increases and heat transfer coefficient decreases with increasing pressure, similar to the trend observed in Gang et al. [30] and Tanimizu and Sadr [8]. The reason is that near the pseudo-critical temperature, the specific heat capacity of the fluid decreases with pressure, which reduces the heat absorbing ability of the fluid. Near the outlet of the tube, the heat transfer coefficient shows negligible dependence on pressure, as the fluid temperature is far from the pseudocritical temperature and thus pressure has a small effect on the thermophysical properties. Similar trends of dependence on pressure are also reported in Refs. [40–42]. The heat transfer coefficient along the tube for pressure of 20.15 MPa is in general higher than the values for all other pressures and does not follow the pressure dependence described above. It is worth noting that most existing literature for sCO_2 heat transfer focused on the pressure range below 15 MPa, and the heat transfer performance of sCO_2 at such high pressure has not been reported before and compared with other pressure conditions. Here, we provide our hypothesis on the observed behavior. The reason for the high heat transfer coefficient for 20.15 MPa condition is likely because at very high pressure far above the critical pressure, near the pseudo-critical temperature, the variation of the thermophysical properties of fluid is small, so the heat transfer behavior is close to single-phase fluid convection, and flow stratification is less likely to occur. On the contrary, for lower supercritical pressures, the variation of fluid thermophysical properties is more dramatic near the pseudo-critical point, so that the near wall region is easily accumulated by higher temperature fluid with small thermal

conductivity and specific heat capacity, which results in heat transfer deterioration [21]. Moreover, as discussed before, for low supercritical pressure conditions, the flow is more easily stratified, which results in reduced heat transfer at the top generatrix. In the high enthalpy region near the outlet of the tube, the fluid thermal conductivity is also higher at high pressure, resulting in enhanced heat transfer ability.

Effect of mass flux

Figure 7 shows the circumferential average wall temperature and heat transfer coefficient with different mass fluxes under four different pressure conditions. Figure 7a and b correspond to a subcritical pressure (6.03 MPa), Figure 7c and d correspond to a near-critical pressure (7.31 MPa), Figure 7e and f correspond to a low supercritical pressure (7.61 MPa), and Figure 7g and h correspond to a high supercritical pressure (20.20 MPa). For subcritical pressure far from the critical pressure, higher mass flux results in smaller wall temperature peak due to the larger inertia force to prevent vapor film expansion near the wall [43]. The location of the wall temperature peak shifts toward smaller enthalpy value with increasing mass flux, which agrees with the flow regime map of Cheng et al. [26, 27] and is consistent with previous experimental observations [44, 45]. The heat transfer coefficient is insensitive to the variation of mass flux, similar to the trend observed in Refs. [25, 38, 44], which is because boiling characteristics dominate heat transfer, which is more sensitive to bubble dynamics, especially in the nucleate boiling regime. For other pressures shown by Figure 7c–h, the general trend is that the heat transfer coefficient increases with mass flux, as expected since higher mass flux results in larger *Re* and higher turbulence. The effect of mass flux is less prominent for lower pressures (Figure 7c and f) while more prominent for high pressures (Figure 7g and h), which is possibly because for high pressure conditions, the heat transfer is very close to single-phase convection due to the small variation of thermophysical properties, which is dominated by *Re*.

Effect of heat flux

Figure 8 shows the circumferential average wall temperature and heat transfer coefficient with different heat flux under different pressure conditions. Figure 8a and b correspond to a subcritical pressure (6.02 MPa), Figure 8c and d correspond to a near-critical pressure (7.32 MPa), Figure 8e and f correspond to a low supercritical pressure (7.62 MPa), and Figure 8g and h correspond to a high supercritical pressure (20.23 MPa).

As shown in Figure 8a and b, under subcritical pressure, the magnitude of the wall temperature peak increases with increasing heat flux, as expected. The heat transfer coefficient in the low enthalpy region increases with heat flux, which is because nucleate boiling dominates this regime and higher heat flux enhances bubble dynamics and improves nucleate boiling heat transfer. Similar behavior has been observed in Ref. [38, 46–48]. The sudden rise of the wall temperature due to departure from nucleate boiling shifts toward smaller enthalpy value with increasing heat flux, due to the more efficient bubble generation promoting vapor film formation. In the large enthalpy region (after the wall temperature peak), the heat transfer coefficient is almost independent of heat flux, which can be attributed to the dominance of mist flow in this regime.

Under other pressures, the wall temperature generally increases with increasing heat flux, but the heat transfer coefficient variation is different. For near-critical pressure shown in Figure 8d, before entering the two-phase region (the region between the two dashed lines for saturated liquid and vapor phases), the heat transfer coefficient near the inlet shows negligible dependence on the heat flux, which is because the heat transfer is purely single-phase convection of the liquid phase. Near the two-phase region, the heat transfer coefficient shows a bump, and it increases with increasing heat flux, which can be attributed to the enhanced subcooled boiling with increasing heat flux. Similar phenomenon has been reported in Ref. [39]. For supercritical pressures, the heat transfer coefficient increases with increasing heat flux in the large enthalpy region as shown in Figure 8f and h, which is perhaps due to the enhanced mixing caused by density variation between the near wall fluid and the bulk fluid. In the small enthalpy region, the variation of heat transfer coefficient with heat flux is more complex, showing nearly no variation for low critical pressure (Figure 8f) while non-monotonic variation for high critical pressure (Figure 8h). This can be understood considering the combined effects of various factors: with higher heat flux, the near wall fluid has lower thermal conductivity which impairs heat transfer, the non-equilibrium mixing is enhanced which enhances heat transfer, and the fluid near the pseudocritical point has large specific heat capacity which also enhances heat transfer. Therefore, increasing pressure causes complex enhancement and impairment effects [31, 49] and results in complicated behavior.

Similarity between subcritical and supercritical heat transfer

As mentioned before, there are similarities between subcritical boiling and supercritical heat transfer. The pseudo-boiling concept is developed based on the observation that supercritical fluids possess gas-like (or vapor-like) and liquid-like phases. Recently, Wang et al. [23] proposed a three-regime-model to introduce a two-phase-like regime in supercritical region, further validates the similarity between subcritical boiling and supercritical pseudo-boiling. The three-regime-model for supercritical heat transfer [23] was developed based on analogy with subcritical boiling. However, it is worth mentioning that due to the fundamental differences between these two heat transfer modes. For example, for a given pressure, subcritical boiling occurs under the saturation temperature, while supercritical pseudo-boiling occurs over a finite temperature range. Moreover, the latent heat of subcritical boiling is purely used to expand the intermolecular distance, while the pseudo-boiling enthalpy in supercritical pseudo-boiling contains both latent and sensible parts. Therefore, a unified model covering both modes is currently not available and requires future investigation. In this work, we demonstrate the connection between the two heat transfer modes based on the three-regime-model, in particular, using the pseudo-vapor quality defined in Ref. [23].

In classical subcritical two-phase theory, the thermodynamic equilibrium vapor quality for a two-phase mixture can be calculated as

$$x = \frac{i_b - i_L}{i_V - i_L} \tag{9}$$

where i_b, i_L and i_V are the enthalpy of the bulk fluid, saturated liquid, and saturated vapor, respectively. Similarly, because of the similarity between subcritical boiling and supercritical pseudo-boiling, the pseudo-vapor quality is defined for supercritical conditions in the three-region model [23]

$$x = \frac{i_b - i_{LL}}{i_{VL} - i_{LL}} \tag{10}$$

where i_b, i_{LL} and i_{VL} are the enthalpy of the bulk fluid, liquid-like phase, and vapor-like phase, respectively. The liquid-like and vapor-like fluid enthalpies i_{LL} and i_{VL} are evaluated based on the pseudo-boiling temperatures T^- and T^+ (start and endpoint of the isobaric transition), which are calculated using thermodynamic methods [19]. The pseudo-vapor quality x represents the fluid regime, with $x<0$ representing liquid-like regime, $0<x<1$ representing two-phase-like regime, and $x>1$ representing vapor-like regime.

All the experimental results of this work are then processed using the defined x for both subcritical and supercritical conditions. For each working condition, each of the 19 thermocouple locations represent one data point. Using the local bulk fluid temperature, x can be obtained for each data point. Meanwhile, for each data point, the Nu ratio can be calculated, which is defined as the ratio of Nu_{exp} to Nu_{DB}, with Nu_{exp} and Nu_{DB} being the Nu number obtained experimentally and the Nu number calculated using the classical Dittus-Boelter (DB) correlation, respectively,

$$Nu = \frac{hd_i}{\lambda_b} \tag{11}$$

$$Nu_{DB} = 0.023 Re_b^{0.8} Pr_b^{0.4} \tag{12}$$

where h represents the local heat transfer coefficient for each data point, and λ_b, Re_b, and Pr_b are obtained using the local bulk fluid temperature. For subcritical conditions with the bulk fluid at the saturation temperature (i.e., saturated two-phase mixture), the bulk fluid properties are evaluated as the weighted average of the properties for saturated liquid and saturated vapor, respectively [50]. The applicable parameter ranges of Eq. (12) are $Re_b > 10^4$, $0.7 < Pr_b < 120$ and $L/d > 60$. The experimental parameter ranges of this work are $Re_b = 4.5\times10^4$–5.8×10^5, $Pr_b = 0.74$–46.5, and $L/d = 250$, which is within the applicable conditions of Eq. (12).

Figure 9 shows the Nu ratio as a function of x for all the data points. Clearly, for both subcritical and supercritical pressures, the general trend of the data points are similar. When $x<0$, corresponding to

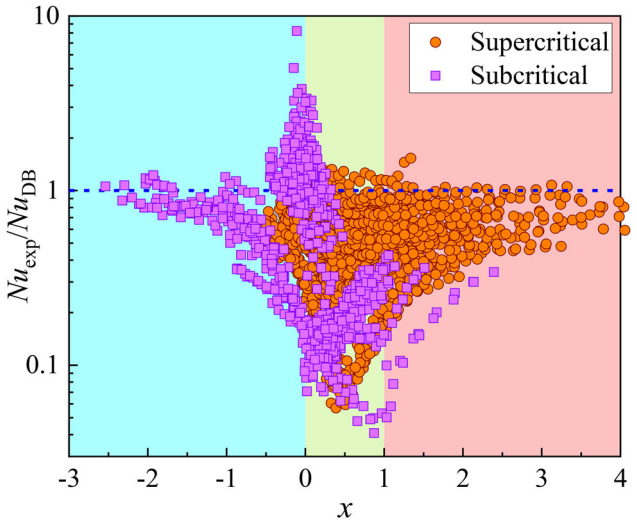

Figure 9. The Nu ratio as a function of vapor quality x for subcritical and supercritical pressures.

subcooled liquid for subcritical pressure and liquid-like regime for supercritical pressure, and when $x > 1$, corresponding to superheated vapor for subcritical pressure and vapor-like regime for supercritical pressure, the *Nu* ratio is close to 1, indicating that heat transfer characteristics are close to single-phase convection. When $0 < x < 1$, corresponding to two-phase mixture for subcritical pressure and two-phase-like regime for supercritical pressure, the *Nu* ratio significantly deviates from 1, indicating that the heat transfer characteristics cannot be accurately captured by the single-phase DB correlation.

It is noted that for subcritical pressure, in the two-phase regime with small vapor quality and in the liquid regime adjacent to the two-phase regime, some of the data points have *Nu* ratio significantly above 1, which represent highly efficient nucleate boiling (including subcooled boiling) with heat transfer coefficients much greater than those of single-phase convection. However, there are also data points in these regimes with *Nu* ratio below 1, and the reasons are discussed below. For low subcritical pressures (5.5–6.5 MPa), with increasing vapor quality, the bubbles near wall accumulate and cause dry-out, and mist flow is likely to occur at large vapor qualities, which results in significant reduction of heat transfer coefficient, which has also been observed in Ref. [27]. For near-critical pressures (7–7.3 MPa), one possible reason for *Nu* ratio below 1 is that as pressure increases toward the critical point, the specific heats of both saturated liquid and saturated vapor increase significantly, and they attain very large values at near-critical pressure. This causes the calculated Nu_{DB} to be numerically large in the two-phase region, resulting in small *Nu* ratio. Another probable reason is because under high subcritical pressure, the surface tension and the latent heat of liquid are both small, and small bubbles are easily generated, which tend to form a vapor film, causing the heat transfer to be impaired, and heat transfer coefficient shows a sudden decrease corresponding to departure from nucleate boiling even when the bulk fluid is subcooled, resulting in heat transfer performance worse than single-phase convection, as reported in Ref. [39]. For supercritical heat transfer, many data points also have *Nu* ratio below 1. The main reason is similar to near-critical pressure conditions: near the pseudo-critical temperature, the fluid specific heat increases dramatically and reaches a peak, causing large calculated Nu_{DB} and small *Nu* ratio [51]. Another possible reason is that due to the sharp variation of thermophysical properties, the near wall region is occupied by fluid with small thermal conductivity which impairs heat transfer, resulting in heat transfer deterioration [21].

We quantify the deviation of Nu_{exp} from Nu_{DB} by calculating the relative errors of the data points in different regimes, including the mean relative error e_A, the mean absolute relative error e_R, and the root-mean-square relative error e_S, defined as follows:

$$e_A = \frac{1}{n}\sum_{i=1}^{n} e_i, e_R = \frac{1}{n}\sum_{i=1}^{n} |e_i|, e_S = \sqrt{\frac{1}{n}\sum_{i=1}^{n} e_i^2} \quad (13)$$

where

$$e_i = \frac{Nu_{DB} - Nu_{exp}}{Nu_{exp}} \quad (14)$$

The calculated errors are as follows: in the liquid/liquid-like regime ($x < 1$), e_A = 70%, e_R = 84%, and e_S = 142%; in the two-phase/two-phase-like regime ($0 < x < 1$), e_A = 274%, e_R = 278%, and e_S = 429%; in the vapor/vapor-like regime ($x > 1$), e_A = 128%, e_R = 129%, and e_S = 223%. The two-phase/two-phase-like regime shows much greater errors compared to single-phase regimes.

The reason for the trends observed above is that for subcritical conditions, the occurrence of boiling produce complex two-phase flow characteristics that cannot be treated as single-phase; similarly, for supercritical conditions, the two-phase-like regime can be viewed as having a mixture of liquid-like and vapor-like phases, inducing significant deviation from single-phase convection. Of course, the boundaries ($x = 0$ and $x = 1$) do not provide sharp transition, and certain deviation from DB correlation in $x < 0$ and $x > 1$ also exists, especially near the boundaries, which is because of the non-equilibrium heat transfer characteristics such as subcooled boiling, as well as the error from the DB correlation itself. It is noted that due to the intrinsic inaccuracy of DB correlation in characterizing subcritical flow boiling and supercritical heat transfer, the errors calculated above are not meant to recommend the utilization of DB correlation, but to demonstrate that compared to the single-phase regimes, the errors are relatively larger in the two-phase/two-phase-like regimes. The trend observed in Figure 9 verifies the similarity in subcritical boiling and supercritical pseudo-boiling.

Summary and conclusions

In this work, we conducted experimental investigation on the heat transfer characteristics of CO_2 heated in a horizontal circular tube under both subcritical and supercritical pressures over a wide range of operation

parameters. The effects of pressure, mass flux, and heat flux on the heat transfer characteristics are discussed. The similarities between subcritical and supercritical heat transfer have been demonstrated using the vapor quality and its counterpart defined in the three-regime-model. The main conclusions of this work include:

1. Under subcritical pressure far below the critical pressure, the heat transfer shows classical flow boiling characteristics. The wall temperature shows a peak corresponding to departure from nucleate boiling, and high heat transfer coefficient is obtained at small vapor quality due to efficient nucleate boiling. Under near-critical pressures, the heat transfer characteristics are similar to those at critical pressures. The wall temperature increases smoothly along the tube and decreases from the top to the bottom of the tube along the circumferential direction.
2. With increasing pressure, the heat transfer coefficient decreases for subcritical pressure far below critical pressure. Similar trend can also be observed for supercritical conditions, except for the highest pressure of 20.15 MPa which shows the largest heat transfer coefficient. The reason can be attributed to the insignificant variation of thermophysical properties at high supercritical pressure, avoiding the accumulation of low thermal conductivity fluid near the wall.
3. Under subcritical pressure far below the critical pressure, the heat transfer coefficient does not vary too much with mass flux, because nucleate boiling dominates heat transfer. Under other pressures, the heat transfer coefficient increases with increasing mass flux due to the enhanced turbulence.
4. Under subcritical pressure far below the critical pressure, the heat transfer coefficient increases with increasing heat flux in the nucleate boiling regime and does not vary with heat flux in the mist flow regime. Under other pressures, the heat transfer coefficient generally increases with heat flux, but the variation is rather complicated due to the combination of different effects.
5. Using the pseudo-vapor quality concept introduced by the three-regime-model, the heat transfer coefficient is found to be very similar between subcritical and supercritical conditions. The errors for experimental Nu number deviating from single-phase DB correlation are much larger in the two-phase/two-phase-like regime compared to those in the liquid/-liquid-like and vapor/vapor-like regime, indicating that the two-phase/two-phase-like regime is dominated by boiling/pseudo-boiling characteristics and deviates from single-phase convection, which validates the similarity between subcritical boiling and supercritical pseudo-boiling.

Funding

This work is supported by National Natural Science Foundation of China (Grant No. 52106198), Beijing Natural Science Foundation (Grant No. 3222047), and Beijing Nova Program (Z211100002121158).

Notes on contributors

Chengrui Zhang is a master student in North China Electric Power University, majoring in power engineering and engineering thermophysics. He received his bachelor's degree in engineering from Anhui University of Science and Technology. He is currently working in the Beijing Key Laboratory of Multiphase Flow and Heat Transfer for Low Grade Energy Utilization. He is devoted to the experimental investigation of supercritical carbon dioxide heat transfer.

Bingtao Hao is a master student in the School of Energy, Power, and Mechanical Engineering at North China Electric Power University. He received his bachelor's degree from Harbin University of Commerce. He is working in the Beijing Key Laboratory of Multiphase Flow and Heat Transfer for Low Grade Energy Utilization on flow and heat transfer of supercritical carbon dioxide.

Liangyuan Cheng is a doctoral candidate in North China Electric Power University, majoring in power engineering and engineering thermophysics, He received his master's degree in Northeast Electric Power University and his bachelor's degree in Shenyang institute of Engineering. He is working in the Beijing Key Laboratory of Multiphase Flow and Heat Transfer for Low Grade Energy Utilization. He is devoted to the experimental investigation of supercritical carbon dioxide heat transfer.

Jinliang Xu is a Professor at the School of Energy Power and Mechanical Engineering, North China Electric Power University. He is currently the Director of Beijing Key Laboratory of Multiphase Flow and Heat Transfer for Low Grade Energy Utilization. His research interest

includes multiphase flow and heat transfer in micro/nano systems, advanced power generation system, low grade energy and renewable energy utilization. He has published over 200 international journal papers as corresponding author and coauthored two books. He has been the chair or co-chair for multiple international conferences, the editor or associate editor of multiple journals including Energies, Thermal Science and Engineering Progress, Frontiers in Heat pipe, and Alternative Energy, and the guest editor for the special issue of Applied Thermal Engineering and Energy. He has presented over 40 keynote speeches in international conferences and has been the reviewer for more than 30 journals. He received the Natural Science Award of the Ministry of Education, China (first grade) in 2012. He has been the "973" project chief scientist, Ministry of Science in 2011 and was awarded as "Yangtze River Scholar" Professor by the National Ministry of education, China in 2013.

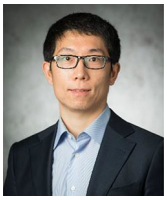

Qingyang Wang is an Associate Professor in the School of Energy Power and Mechanical Engineering at North China Electric Power University. He obtained his B.Eng. in energy power system and automation from Tsinghua University in 2015, and Ph.D. in mechanical engineering from University of California San Diego in 2020. His research interests include micro/nanoscale heat transfer, phase change heat transfer and multiphase flow, and supercritical energy transport and conversion.

References

[1] M. Herrero, J. A. Mendiola, A. Cifuentes and E. Ibanez, "Supercritical fluid extraction: Recent advances and applications," *J. Chromatogr. A.*, vol. 1217, no. 16, pp. 2495–2511, 2010. DOI: 10.1016/j.chroma.2009.12.019.

[2] F. Eskandari Manjili and M. Cheraghi, "Performance of a new two-stage transcritical CO_2 refrigeration cycle with two ejectors," *Appl. Therm. Eng.*, vol. 156, pp. 402–409, Jun. 2019. DOI: 10.1016/j.applthermaleng.2019.03.083.

[3] T. Tamura, Y. Yakumaru and F. Nishiwaki, "Experimental study on automotive cooling and heating air conditioning system using CO_2 as a refrigerant," *Int. J. Heat Mass Transf.*, vol. 28, no. 8, pp. 1302–1307, 2005. DOI: 10.1016/j.ijrefrig.2005.09.010.

[4] P. Byrne, J. Miriel and Y. Lenat, "Design and simulation of a heat pump for simultaneous heating and cooling using HFC or CO_2 as a working fluid," *Int. J. Refrig.*, vol. 32, no. 7, pp. 1711–1723, 2009. DOI: 10.1016/j.ijrefrig.2009.05.008.

[5] V. Dostal, P. Hejzlar and M. J. Driscoll, "The supercritical carbon dioxide power cycle: Comparison to other advanced power cycles," *Nucl. Technol.*, vol. 154, no. 3, pp. 283–301, 2006. DOI: 10.13182/NT06-A3734.

[6] Q. Wang, J. Xu, C. Zhang, B. Hao and L. Cheng, "A critical review on heat transfer of supercritical fluids," *Heat Transf. Eng.*, 2023. DOI: 10.1080/01457632.2022.2164684.

[7] G. A. Adebiyi and W. B. Hall, "Experimental investigation of heat transfer to supercritical pressure carbon dioxide in a horizontal pipe," *Int. J. Heat Mass Transf.*, vol. 19, no. 7, pp. 715–720, 1976. DOI: 10.1016/0017-9310(76)90123-X.

[8] K. Tanimizu and R. Sadr, "Experimental investigation of buoyancy effects on convection heat transfer of supercritical CO_2 flow in a horizontal tube," *Heat Mass. Transf.*, vol. 52, no. 4, pp. 713–726, 2016. DOI: 10.1007/s00231-015-1580-9.

[9] L. Wang, et al., "Experimental investigation in the pressure drop characteristics of supercritical carbon dioxide in the uniformly heated horizontal miniature tubes," *J. Supercrit. Fluids.*, vol. 162, pp. 104839, Aug. 2020. DOI: 10.1016/j.supflu.2020.104839.

[10] T. H. Kim, J. G. Kwon, M. H. Kim and H. S. Park, "Experimental investigation on validity of buoyancy parameters to heat transfer of CO_2 at supercritical pressures in a horizontal tube," *Exp. Therm. Fluid Sci.*, vol. 92, pp. 222–230, Apr. 2018. DOI: 10.1016/j.expthermflusci.2017.11.024.

[11] J. Wang, et al., "Computational investigations of heat transfer to supercritical CO_2 in a large horizontal tube," *Energy Convers. Manag.*, vol. 157, pp. 536–548, Feb. 2018. DOI: 10.1016/j.enconman.2017.12.046.

[12] X. Chu and E. Laurien, "Flow stratification of supercritical CO_2 in a heated horizontal pipe," *J. Supercrit. Fluid.*, vol. 116, pp. 172–189, Oct. 2016. DOI: 10.1016/j.supflu.2016.05.003.

[13] H. Zhang, J. Guo, X. Cui and X. Huai, "Heat transfer performance of supercritical pressure CO_2 in a non-uniformly heated horizontal tube," *Int. J. Heat Mass Transf.*, vol. 155, pp. 119748, Jul. 2020. DOI: 10.1016/j.ijheatmasstransfer.2020.119748.

[14] C.-S. Yan and J.-L. Xu, "Numerical analysis on flow and heat transfer of supercritical CO_2 in horizontal tube," *Acta Phys. Sin.*, vol. 69, no. 4, pp. 044401, Jan. 2020. DOI: 10.7498/aps.69.20191513.

[15] P. Gallo, D. Corradini and M. Rovere, "Widom line and dynamical crossovers as routes to understand supercritical water," *Nat Commun*, vol. 5, no. 1, pp. 5806, 2014. DOI: 10.1038/ncomms6806.

[16] G. G. Simeoni, et al., "The widom line as the crossover between liquid-like and gas-like behaviour in supercritical fluids," *Nature Phys.*, vol. 6, no. 7, pp. 503–507, 2010. DOI: 10.1038/nphys1683.

[17] F. Maxim, et al., "Visualization of supercritical water pseudo-boiling at widom line crossover," *Nat. Commun.*, vol. 10, no. 1, pp. 4114, Sep. 2019. DOI: 10.1038/s41467-019-12117-5.

[18] F. Maxim, et al., "Thermodynamics and dynamics of supercritical water pseudo-boiling," *Adv. Sci. (Weinh).*, vol. 8, no. 3, pp. 2002312, Feb. 2021. DOI: 10.1002/advs.202002312.

[19] D. T. Banuti, "Crossing the widom-line - supercritical pseudo-boiling," *J. Supercrit. Fluid.*, vol. 98, pp. 12–16, Mar. 2015. DOI: 10.1016/j.supflu.2014.12.019.

[20] M. Y. Ha, T. J. Yoon, T. Tlusty, Y. Jho and W. B. Lee, "Widom delta of supercritical gas-liquid coexistence," *J. Phys. Chem. Lett.*, vol. 9, no. 7, pp. 1734–1738, 2018. DOI: 10.1021/acs.jpclett.8b00430.

[21] B. G. Zhu, J. L. Xu, X. M. Wu, J. Xie and M. J. Li, "Supercritical boiling' number, a new parameter to distinguish two regimes of carbon dioxide heat transfer in tubes," *Int. J. Therm. Sci.*, vol. 136, pp. 254–266, Feb. 2019. DOI: 10.1016/j.ijthermalsci.2018.10.032.

[22] B. G. Zhu, J. L. Xu, C. S. Yan and J. Xie, "The general supercritical heat transfer correlation for vertical up-flow tubes: K number correlation," *Int. J. Heat Mass Transf.*, vol. 148, no. 8, pp. 119080, Feb. 2020. DOI: 10.1016/j.ijheatmasstransfer.2019.119080.

[23] Q. Wang, X. Ma, J. Xu, M. Li and Y. Wang, "The three-regime-model for pseudo-boiling in supercritical pressure," *Int. J. Heat Mass Transf.*, vol. 181, pp. 121875, Dec. 2021. DOI: 10.1016/j.ijheatmasstransfer.2021.121875.

[24] R. Yun, Y. Kim, M. Soo Kim and Y. Choi, "Boiling heat transfer and dryout phenomenon of CO_2 in a horizontal smooth tube," *Int. J. Heat Mass Transf.*, vol. 46, no. 13, pp. 2353–2361, 2003. DOI: 10.1016/S0017-9310(02)00540-9.

[25] M. Ducoulombier, S. Colasson, J. Bonjour and P. Haberschill, "Carbon dioxide flow boiling in a single microchannel – Part II: Heat transfer," *Exp. Therm. Fluid Sci.*, vol. 35, no. 4, pp. 597–611, 2011. DOI: 10.1016/j.expthermflusci.2010.11.014.

[26] L. Cheng, G. Ribatski, J. Moreno Quibén and J. R. Thome, "New prediction methods for CO_2 evaporation inside tubes: Part I – A two-phase flow pattern map and a flow pattern based phenomenological model for two-phase flow frictional pressure drops," *Int. J. Heat Mass Transf.*, vol. 51, no. 1–2, pp. 111–124, 2008. DOI: 10.1016/j.ijheatmasstransfer.2007.04.002.

[27] L. Cheng, G. Ribatski and J. R. Thome, "New prediction methods for CO_2 evaporation inside tubes: Part II—An updated general flow boiling heat transfer model based on flow patterns," *Int. J. Heat Mass Transf.*, vol. 51, no. 1-2, pp. 125–135, 2008. DOI: 10.1016/j.ijheatmasstransfer.2007.04.001.

[28] L. Cheng, G. Xia and Q. Li, "CO_2 Evaporation process modeling: Fundamentals and engineering applications," *Heat Transf. Eng.*, vol. 43, no. 8-10, pp. 658–678, 2022. DOI: 10.1080/01457632.2021.1905297.

[29] L. Jiang, J. Liu, L. Zhang and X. Xu, "A research on the dryout characteristics of CO_2'S flow boiling heat transfer process in mini-channels," *Int. J. Refrig.*, vol. 83, pp. 131–142, Nov. 2017. DOI: 10.1016/j.ijrefrig.2017.07.017.

[30] W. Gang, et al., "Forced convection heat transfer using high temperature and pressure water in an upward-inclined tube," *J. Heat. Trans-T ASME.*, vol. 134, no. 2, pp. 020905, 2012. DOI: 10.1115/1.4004901.

[31] S. Wang, D. Yang, B. Xie, L. Wang and Y. Wang, "Experimental investigation on heat transfer characteristics of water in inclined downward tube of a supercritical pressure CFB boiler," *J. Therm. Sci.*, vol. 24, no. 5, pp. 478–487, 2015. DOI: 10.1007/s11630-015-0811-1.

[32] X. Zhu, Q. Bi, D. Yang and T. Chen, "An investigation on heat transfer characteristics of different pressure steam-water in vertical upward tube," *Nucl. Eng. Des.*, vol. 239, no. 2, pp. 381–388, Feb. 2009. DOI: 10.1016/j.nucengdes.2008.10.026.

[33] J. Wang, H. Li, S. Yu and T. Chen, "Comparison of the heat transfer characteristics of supercritical pressure water to that of subcritical pressure water in vertically-upward tubes," *Int. J. Multiph. Flow*, vol. 37, no. 7, pp. 769–776, 2011. DOI: 10.1016/j.ijmultiphaseflow.2011.01.013.

[34] X. Lei, R. Peng, Z. Guo, H. Li, K. Ali and X. Zhou, "Experimental comparison of the heat transfer of carbon dioxide under subcritical and supercritical pressures," *Int. J. Heat Mass Transf.*, vol. 152, pp. 119562, May 2020. DOI: 10.1016/j.ijheatmasstransfer.2020.119562.

[35] H. Zhang, J. Xu, Q. Wang and X. Zhu, "Multiple wall temperature peaks during forced convective heat transfer of supercritical carbon dioxide in tubes," *Int. J. Heat Mass Transf.*, vol. 172, pp. 121171, Jun. 2021. DOI: 10.1016/j.ijheatmasstransfer.2021.121171.

[36] E. W. Lemmon, M. L. Huber and M. O. Mc Linden, "NIST Standard Reference Database 23: Reference fluid thermodynamic and transport properties-REFPROP, Version 9.1," Technical Report, National Institute of Standards and Technology, Standard Reference Data Program, Gaithersburg, 2013.

[37] D. Hellenschmidt and P. Petagna, "Effects of saturation temperature on the boiling properties of carbon dioxide in small diameter pipes at low vapour quality: Heat transfer coefficient," *Int. J. Heat Mass Transf.*, vol. 172, pp. 121094, Jun. 2021. DOI: 10.1016/j.ijheatmasstransfer.2021.121094.

[38] H.-K. Oh and C.-H. Son, "Flow boiling heat transfer and pressure drop characteristics of CO_2 in horizontal tube of 4.57-mm inner diameter," *Appl. Therm. Eng.*, vol. 31, no. 2-3, pp. 163–172, 2011. DOI: 10.1016/j.applthermaleng.2010.08.026.

[39] X. Lei, W. Zhang, J. Zhang, N. Dinh and H. Li, "Experimental investigations on the boiling heat transfer of horizontal flow in the near-critical region," *Int. J. Heat Mass Transf.*, vol. 125, pp. 618–628, Oct. 2018. DOI: 10.1016/j.ijheatmasstransfer.2018.04.043.

[40] Z. Shen, et al., "Flow and heat transfer characteristics of high-pressure water flowing in a vertical upward smooth tube at low mass flux conditions," *Appl. Therm. Eng.*, vol. 102, pp. 391–401, Jun. 2016. DOI: 10.1016/j.applthermaleng.2016.03.150.

[41] A. Taklifi, P. Hanafizadeh, M. A. A. Behabadi and A. Aliabadi, "Experimental investigation on heat transfer and pressure drop of supercritical water flows in an inclined rifled tube," *J. Supercrit. Fluid.*, vol. 107, pp. 209–218, Jan. 2016. DOI: 10.1016/j.supflu.2015.09.011.

[42] Q. Zhang, H. Li, X. Kong, J. Liu and X. Lei, "Special heat transfer characteristics of supercritical CO_2 flowing in a vertically-upward tube with low mass flux," *Int. J. Heat Mass Transf.*, vol. 122, pp. 469–482, Jul. 2018. DOI: 10.1016/j.ijheatmasstransfer.2018.01.112.

[43] S. G. Kandlikar, "Evaporation momentum force and its relevance to boiling heat transfer," *J. Heat Transf.*, vol. 142, no. 10, pp. 100801, Oct. 2020. DOI: 10.1115/1.4047268.

[44] R. Mastrullo, A. W. Mauro and L. Viscito, "Flow boiling of carbon dioxide: Heat transfer for smooth and enhanced geometries and effect of oil. state of the art review," *Int. J. Refrig.*, vol. 108, pp. 311–335, Dec. 2019. DOI: 10.1016/j.ijrefrig.2019.08.028.

[45] L. Wojtan, T. Ursenbacher and J. R. Thome, "Investigation of flow boiling in horizontal tubes: Part I—A new diabatic two-phase flow pattern map," *Int. J. Heat Mass Transf.*, vol. 48, no. 14, pp. 2955–2969, 2005. DOI: 10.1016/j.ijheatmasstransfer.2004.12.012.

[46] R. Yun, Y. Kim and M. S. Kim, "Flow boiling heat transfer of carbon dioxide in horizontal mini tubes," *Int. J. Heat Fluid Flow.*, vol. 26, no. 5, pp. 801–809, 2005. DOI: 10.1016/j.ijheatfluidflow.2005.01.004.

[47] X. Huai, et al., "An experimental study of flow boiling characteristics of carbon dioxide in multiport mini channels," *Appl. Therm. Eng.*, vol. 24, no. 10, pp. 1443–1463, Jul. 2004. DOI: 10.1016/j.applthermaleng.2003.10.032.

[48] K.-I. Choi, A. S. Pamitran and J.-T. Oh, "Two-phase flow heat transfer of CO_2 vaporization in smooth horizontal minichannels," *Int. J. Refrig.*, vol. 30, no. 5, pp. 767–777, 2007. DOI: 10.1016/j.ijrefrig.2006.12.006.

[49] D. Huang, Z. Wu, B. Sunden and W. Li, "A brief review on convection heat transfer of fluids at supercritical pressures in tubes and the recent progress," *Appl. Energy.*, vol. 162, pp. 494–505, Jan. 2016. DOI: 10.1016/j.apenergy.2015.10.080.

[50] V. P. Carey, Liquid Vapor Phase Change Phenomena: An Introduction to the Thermophysics of Vaporization and Condensation Processes in Heat Transfer Equipment (2nd edition), Taylor & Francis Group, New York, 2008.

[51] Q. Zhang, H. Li, X. Lei, J. Zhang and X. Kong, "Study on identification method of heat transfer deterioration of supercritical fluids in vertically heated tubes," *Int. J. Heat Mass Transf*, vol. 127, no. part B, pp. 674–686, Dec. 2018. DOI: 10.1016/j.ijheatmasstransfer.2018.07.058.